Volume 53
Number 20
28 May 2024
Pages 8499-8858

Dalton Transactions

An international journal of inorganic chemistry

rsc.li/dalton

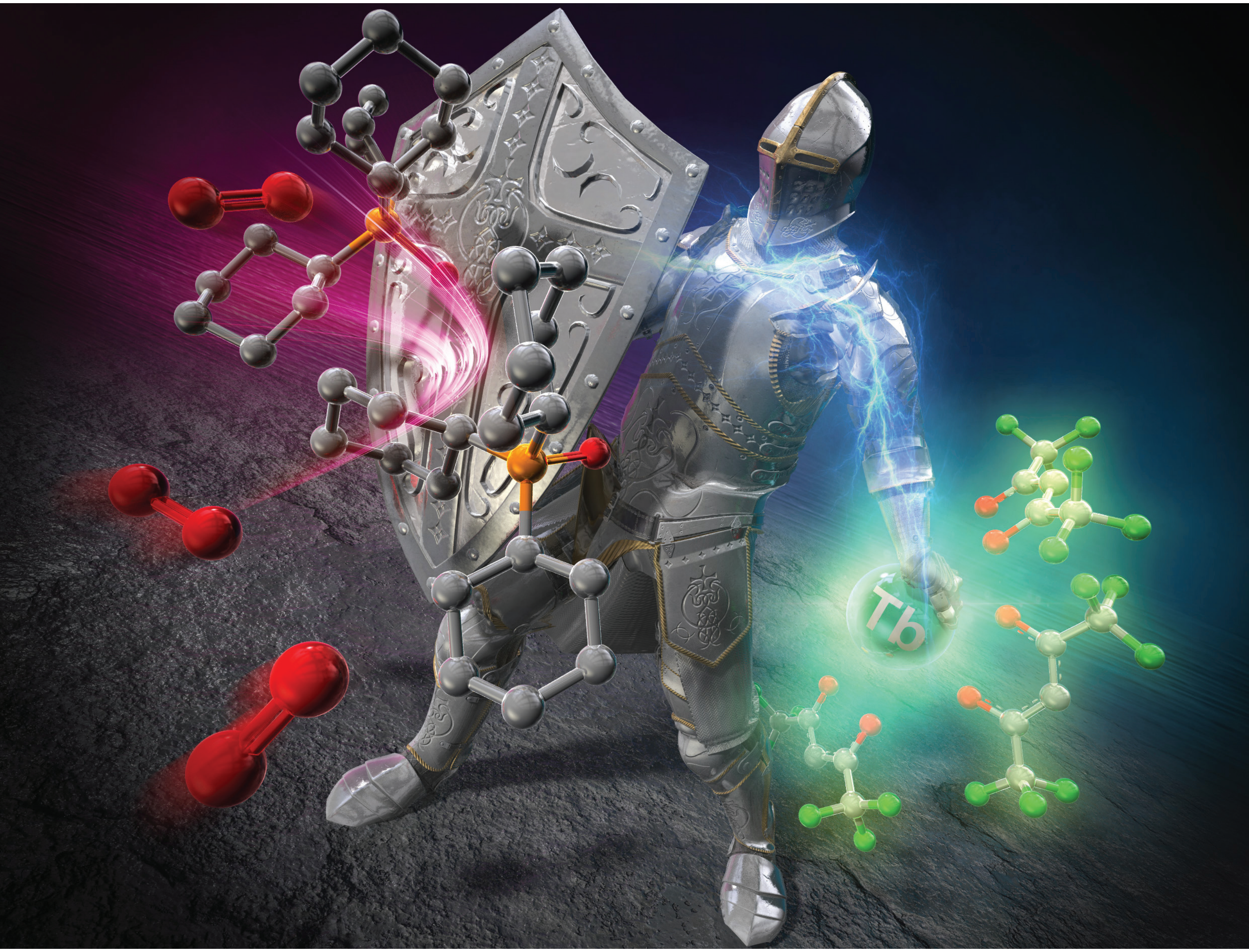

ISSN 1477-9226

ROYAL SOCIETY
OF **CHEMISTRY**

PAPER
Yuichi Kitagawa *et al.*
Effective photosensitized emission of a Tb(III) complex using a β-diketonate photosensitizer and an oxygen barrier system in a thermally populated triplet state

Dalton Transactions

ROYAL SOCIETY OF CHEMISTRY

PAPER

View Article Online
View Journal | View Issue

Check for updates

Cite this: *Dalton Trans.*, 2024, **53**, 8555

Effective photosensitized emission of a Tb(III) complex using a β-diketonate photosensitizer and an oxygen barrier system in a thermally populated triplet state†

Kota Inage,[a] Mengfei Wang,[b,c] Yasuchika Hasegawa *[b,c] and Yuichi Kitagawa *[b,c]

Received 31st January 2024,
Accepted 20th March 2024

DOI: 10.1039/d4dt00286e

rsc.li/dalton

Photosensitizer design of luminescent terbium (Tb(III)) complexes with narrow bandwidths is important for advancing luminescent materials. In this study, we report an effective photosensitizer model in a thermally populated lowest excited triplet (T_1) state during Tb(III) emission. The Tb(III) complex comprises a Tb(III) ion (serving as an emission center), hexafluoroacetylacetonates (acting as photosensitizer ligands), and bulky cyclohexyl group-attached phosphine-oxide-type ligands (functioning as an oxygen barrier system). Emission properties including emission and excitation spectra, ligand-excited emission quantum yields, and emission lifetimes were evaluated in the absence and presence of oxygen. Coordination geometry structures were determined through analysing single-crystal structures. The electronic structure based on 4f-orbitals was estimated from radiative rate constants and quantum chemical calculations. The bulky phosphine oxide ligand not only provides an oxygen barrier system but also induces an electronic structural modulation based on 4f-orbitals, allowing for effective photosensitized Tb(III) emission in a thermally populated ligand T_1 state in air.

Introduction

Trivalent terbium complexes (Tb(III)) have received considerable attention as green luminescent materials owing to their narrow luminescence bandwidths.[1,2] Their enhanced luminescence properties result from a photosensitization effect based on energy transfer (EnT) from organic ligands to Tb(III).[3] Designing ligands strategically for achieving effective photosensitized emission from Tb(III) complexes is crucial in advancing applications for luminescent materials, including light-emitting diodes,[4–7] sensors,[1,8–13] and security inks.[14–16]

In the photosensitized emission process, the organic ligands undergo intersystem crossing from the lowest excited singlet (S_1) state to the lowest excited triplet (T_1) state upon excitation. Subsequently, the ligands transfer their electronic energy to the Tb(III) emission level ($^5D_4$).[2] Intrinsically long-lived $^5D_4$ states (>0.5 ms) often cause emission quenching through back energy transfer (BEnT) from $^5D_4$ to T_1 states.[2] Latva *et al.* performed photophysical analyses of Tb(III) complexes with amino-carboxylate-type ligands.[17] They empirically determined that a sufficiently higher T_1 level compared to the Tb(III) emission level ($\Delta E_{T1\text{-}5D4}$ > 1850 cm^{-1}) is essential for achieving efficient photosensitized emission. Based on these findings, energy-gap ($\Delta E_{T1\text{-}5D4}$) control has been reported for highly luminescent Tb(III) complexes using benzoate-,[18] β-diketonate-,[19] and bipyridine[20]-type ligands. Recently, the importance of the first excited-state ($^7F_5$ level: 2050 cm^{-1}) population of Tb(III) for energy transfer has been reported.[21,22]

On the other hand, further studies revealed the critical importance of the long-lived T_1 state for overcoming emission quenching by BEnT and achieving efficient photosensitized Tb(III) emission, in situations characterized by a small energy gap (Fig. 1a). The long T_1 lifetime allows for efficient Ln(III) emission in the thermally populated T_1 state.[23] Recently, we demonstrated an effective photosensitization model in the thermally populated T_1 state during Tb(III) emission using a typical β-diketonate (hfa: hexafluoroacetylacetonate, T_1 ~ 22 000 cm^{-1}, $\Delta E_{T1\text{-}5D4}$ ~ 1500 cm^{-1}), with long-lived T_1 state controlled by ancillary phosphine oxide ligands.[24] The photosensitization model with a low T_1 level is beneficial for enhancing the brightness of Tb(III) emission (ESI in ref. 25).[25] However, the emission intensity of the Tb(III) luminophores is

---

[a] *Graduate School of Chemical Sciences and Engineering, Hokkaido University, Sapporo 060-8628, Japan*

[b] *Faculty of Engineering, Hokkaido University, Sapporo 060-8628, Japan. E-mail: y-kitagawa@eng.hokudai.ac.jp, hasegaway@eng.hokudai.ac.jp*

[c] *Institute for Chemical Reaction Design and Discovery (WPI-ICReDD), Hokkaido University, Sapporo 001-0021, Japan*

† Electronic supplementary information (ESI) available. CCDC 2323896, 2324233, 2324192 and 2324895. For ESI and crystallographic data in CIF or other electronic format see DOI: **https://doi.org/10.1039/d4dt00286e**

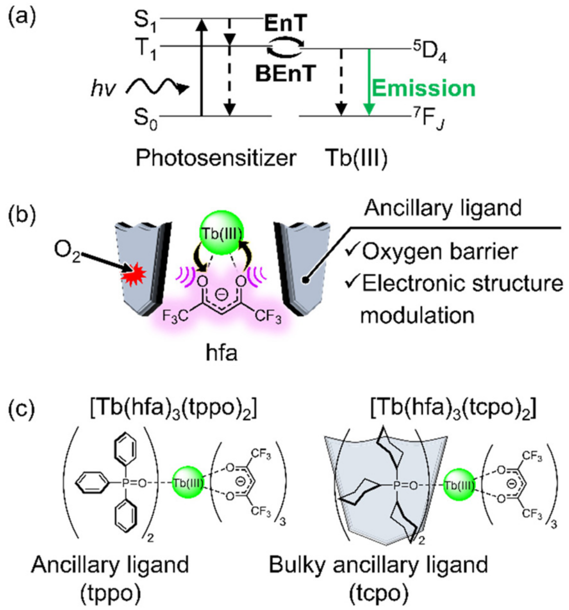

Fig. 1 (a) Excited-state dynamics of luminescent Tb(III) complexes with a small energy gap between T_1 and $^5D_4$ levels (EnT: energy transfer, BEnT: back energy transfer). (b) Illustration of the strategy for highly luminescent Tb(III) complexes under air conditions. (c) Chemical structures of Tb(III) complexes used in this study.

diminished by triplet oxygen quenching when using long-lived T_1 photosensitizers.[10,26–31]

In this study, we report a luminescent Tb(III) complex model using hfa photosensitizer and ancillary ligand with oxygen barrier properties in the solid state (Fig. 1b). A mononuclear Tb(III) complex, [Tb(hfa)$_3$(tcpo)$_2$], was prepared and its photophysical properties were compared to those of [Tb(hfa)$_3$(tppo)$_2$] (Fig. 1c, tppo: triphenylphosphine oxide;[32] tcpo: tricyclohexylphosphine oxide). It was found that the bulky cyclohexyl group not only shields the hfa ligand from oxygen but also provides effective modulation of the 4f-orbital-based electronic structure. Gd(III) complexes were also prepared to estimate the dependence of the T_1 lifetimes on the oxygen concentration. This system provides new insights into the photosensitizer model with a long-lived excited state for highly luminescent Tb(III) complexes in a thermally populated ligand T_1 state in air.

Experimental

Materials

Gadolinium(III) acetate hydrate (99.9%) was purchased from Sigma Aldrich Co., LLC. Terbium(III) acetate tetrahydrate (99.9%) was purchased from FUJIFILM Wako Pure Chemical Corporation. Hexafluoroacetylacetone (>95.0%) and triphenylphosphine oxide (>98.0%) were purchased from Tokyo Chemical Industry Co., Ltd. Tricyclohexylphosphine oxide (>98.0%) was purchased from Kanto Chemical Co., Inc. All other chemicals were reagent grade and used without further purification.

General methods

Electrospray ionization-mass spectrometry (ESI-MS) was performed using a JEOL JMS-T100LP instrument. Elemental analyses were performed using an Exeter Analytical CE440 instrument. Thermogravimetric analyses were performed on a Rigaku Thermo plus EVO2 TG-DTA8122 with Al_2O_3 as a reference. Infrared spectra were measured using a JASCO FT/IR-4600 instrument.

Preparation of [Ln(hfa)$_3$(tppo)$_2$] (Ln = Gd, Tb)

[Ln(hfa)$_3$(tppo)$_2$] was synthesized according to a previously reported method.[32] The mixture of [Ln(hfa)$_3$(H_2O)$_2$] (0.90 mmol) and triphenylphosphine oxide (tppo) (0.5 g, 1.80 mmol) was refluxed at 70 °C in methanol (10 mL) for 3 h. The reaction solution was cooled to approximately 20 °C, and the solvent was distilled using a rotary evaporator. The residue was recrystallized from methanol to produce colorless crystals of the target compounds.

[Gd(hfa)$_3$(tppo)$_2$]. Yield: 0.44 g (37%). MS (ESI) *m/z*: [M − hfa]$^+$ calcd for $C_{46}H_{32}F_{12}GdO_6P_2$ 1128.07; found 1128.06. Anal.: calcd for $C_{51}H_{33}F_{18}GdO_8P_2$: C, 45.89; H, 2.49; found: C, 45.69; H, 2.33%.

[Tb(hfa)$_3$(tppo)$_2$]. Yield: 0.53 g (44%). MS (ESI) *m/z*: [M − hfa]$^+$ calcd for $C_{46}H_{32}F_{12}O_6P_2Tb$ 1129.07; found 1129.06. Anal.: calcd for $C_{51}H_{33}F_{18}O_8P_2Tb$: C, 45.83; H, 2.49; found: C, 45.75; H, 2.35%.

Preparation of [Ln(hfa)$_3$(tcpo)$_2$] (Ln = Gd, Tb)

A mixture of [Ln(hfa)$_3$(H_2O)$_2$] (0.84 mmol) and tricyclohexylphosphine oxide (tcpo) (0.5 g, 1.69 mmol) was refluxed at 70 °C in methanol (10 mL) for 3 h to form a white precipitate. The reaction solution was cooled to approximately 20 °C, and the solvent was distilled using a rotary evaporator. The residue was recrystallized from methanol to produce colorless crystals of the target compounds.

[Gd(hfa)$_3$(tcpo)$_2$]. Yield: 0.80 g (69%). MS (ESI) *m/z*: [M + Na]$^+$ calcd for $C_{51}H_{69}F_{18}GdO_8P_2Na^+$ 1394.33; found 1394.34. Anal.: calcd for $C_{51}H_{69}F_{18}GdO_8P_2$: C, 44.67; H, 5.07; found C, 44.59; H, 4.98%.

[Tb(hfa)$_3$(tcpo)$_2$]. Yield: 0.68 g (58%). MS (ESI) *m/z*: [M + Na]$^+$ calcd for $C_{51}H_{69}F_{18}O_8P_2TbNa^+$ 1395.33; found 1395.33. Anal.: calcd for $C_{51}H_{69}F_{18}O_8P_2Tb$: C, 44.62; H, 5.07; found: C, 44.59; H, 5.02%.

Crystallography

Rigaku MicroMax-007HF with Rigaku HyPix-6000HE and VariMax DW (Mo-Kα radiation (λ = 0.71073 nm)) was used for collecting crystallographic data for Tb(III) and Gd(III) complexes. All calculations were performed using Olex2 except for refinement.[33] Non-hydrogen atoms were refined anisotropically using the SHELX system.[34] Hydrogen atoms were refined using the riding model. CIF files are available in CCDC 2323896 (for Tb(hfa)$_3$(tppo)$_2$), CCDC 2324233 (for Tb

$(hfa)_3(tcpo)_2$), CCDC 2324192 (for $Gd(hfa)_3(tppo)_2$), and CCDC 2324895 (for $Gd(hfa)_3(tcpo)_2$).†

Optical measurements

All optical measurements were carried out in the solid state. Emission and excitation spectra and emission decay profiles of Tb(III) complexes were recorded on a HORIBA Fluorolog-3 spectrofluorometer with a cryostat (Thermal Block Company, SA-SB1905HA, vacuum ultimate pressure of the vacuum pump: 6.7×10^{-2} Pa). For emission decay profiles of Tb(III) complexes, a SpectraLED-355 (λ_{ex} = 356 nm, full width at half maximum (FWHM) = 17 nm) was used as an excitation source. Emission decay profiles of Gd(III) complexes were measured using third-harmonics of a Q-switched Nd:YAG laser (SpectraPhysics, INDI-50, FWHM = 5 ns, λ = 1064 nm) and a photomultiplier (Hamamatsu Photonics, R5108, response time < 1.1 ns). The Nd:YAG laser response was monitored with a digital oscilloscope (Sony Tektronix, TDS3052). Phosphorescence spectra of Gd(III) complexes and emission quantum yields of Tb(III) complexes were measured on a JASCO FP-6300 instrument. A cryostat (Thermal Block Company, SA-SB1905HA) was used for the phosphorescence spectra of Gd(III) complexes. A JASCO ILF-533 integrating sphere unit was used for emission quantum yields of Tb(III) complexes.

Computational details

All quantum chemical calculations were performed using density functional theory (DFT) using the Gaussian 16 package.[35] Energy calculations of Tb(III) complexes were evaluated with the long-range corrected BLYP functional (basis set: Stuttgart RSC 1997 for Tb atoms and cc-pVDZ for C, H, O, F, and P atoms).[36–38]

Results and discussion

Structures of $[Tb(hfa)_3(tppo)_2]$ and $[Tb(hfa)_3(tcpo)_2]$

$[Tb(hfa)_3(tppo)_2]$ and $[Tb(hfa)_3(tcpo)_2]$ were synthesized through refluxing the precursor complex $[Tb(hfa)_3(H_2O)_2]$ with the respective phosphine oxide ligand in methanol. Single crystals of Tb(III) complexes were obtained through recrystallization from methanol. The crystal structures of the complexes are shown in Fig. 2 and their corresponding crystal data are presented in Table 1. Both Tb(III) complexes exhibited eight-coordination structures with three hfa ligands and two phosphine oxide ligands. In both $[Tb(hfa)_3(tppo)_2]$ and $[Tb(hfa)_3(tcpo)_2]$, multiple intra- and intermolecular CH/F interactions were observed. The rigid structures are linked to high thermostability (decomposition point >260 °C, Fig. S1†). In $[Tb(hfa)_3(tcpo)_2]$, two phosphine oxide ligands were located on the same side of the mononuclear complex as bidentate ligands (Fig. 2b),[39] which is distinct from the crystal structure of $[Tb(hfa)_3(tppo)_2]$ (Fig. 2a). We performed continuous shape measure (CShM) analysis to elucidate the coordination geometry of the unit.[40–42] The CShM factor S was calculated to quantitatively estimate the coordination geometry. Based on CShM analysis, the polyhedral structures of $[Tb(hfa)_3(tppo)_2]$ and $[Tb(hfa)_3(tcpo)_2]$ were classified as square antiprism (SAPR) and bicapped trigonal prism (BTPR) structures, respectively (Fig. 2, Table S1†). Additionally, Gd(III) complexes were prepared using the same procedure as that for the Tb(III) complexes. The crystal structures of $[Gd(hfa)_3(tppo)_2]$ and $[Gd(hfa)_3(tcpo)_2]$ closely resembled those of $[Tb(hfa)_3(tppo)_2]$ and $[Tb(hfa)_3(tcpo)_2]$, respectively (Fig. S2, Table S2†)

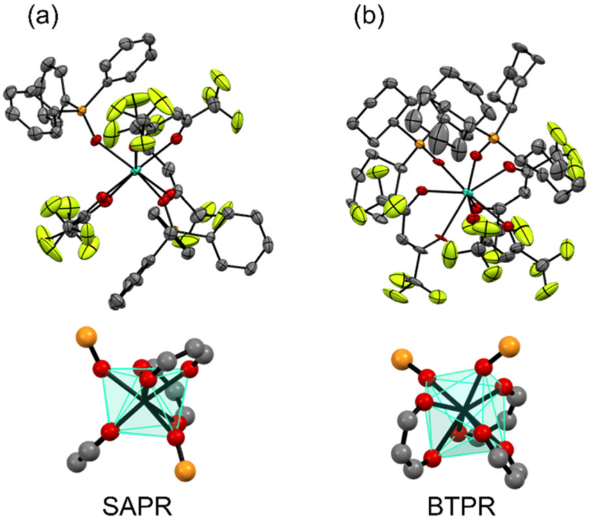

Fig. 2 ORTEP drawings (top) and coordination geometries (bottom) of the Tb(III) complexes: (a) $[Tb(hfa)_3(tppo)_2]$ and (b) $[Tb(hfa)_3(tcpo)_2]$. Ellipsoid probability was set at 50%. Hydrogen atoms are omitted for clarity.

Table 1 Crystal data of $[Tb(hfa)_3(tppo)_2]$ and $[Tb(hfa)_3(tcpo)_2]$

	$[Tb(hfa)_3(tppo)_2]$	$[Tb(hfa)_3(tcpo)_2]$
Chemical formula	$C_{51}H_{33}F_{18}O_8P_2Tb$	$C_{51}H_{69}F_{18}O_8P_2Tb$
Molecular weight	1336.63	1372.92
Crystal system	Monoclinic	Orthorhombic
Space group	$P2_1/n$	$Pca2_1$
a/Å	17.0264(3)	17.9100(6)
b/Å	15.4243(3)	18.7471(6)
c/Å	20.4521(4)	17.3371(5)
α/°	90	90
β/°	93.879(2)	90
γ/°	90	90
Volume/Å^3	5358.83(18)	5821.1(3)
Z	4	4
Density/g cm^{-3}	1.657	1.567
Temperature/°C	−150	−150
R_1	0.0400	0.0804
wR_2	0.0937	0.2366

General photophysical properties

General photophysical properties of $[Tb(hfa)_3(tppo)_2]$ and $[Tb(hfa)_3(tcpo)_2]$ (solid state) were measured in air. Emission, excitation, and diffuse reflectance spectra of the Tb(III) complexes are shown in Fig. 3. Sharp emission bands were observed at around 490, 550, 580, 620, and 650 nm, which are attributed to the $^5D_4 \rightarrow {}^7F_J$ (J = 6, 5, 4, 3, 2) transition of Tb(III), respect-

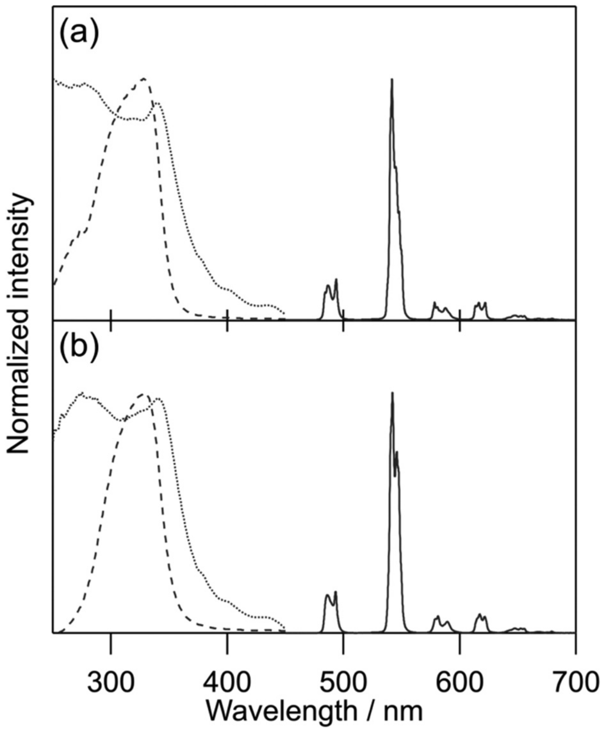

Fig. 3 Emission (solid line, λ_{ex} = 360 nm), excitation (dotted line, λ_{em} = 542 nm), and diffuse reflectance (dashed line) spectra of Tb(III) complexes in air: (a) [Tb(hfa)$_3$(tppo)$_2$] and (b) [Tb(hfa)$_3$(tcpo)$_2$].

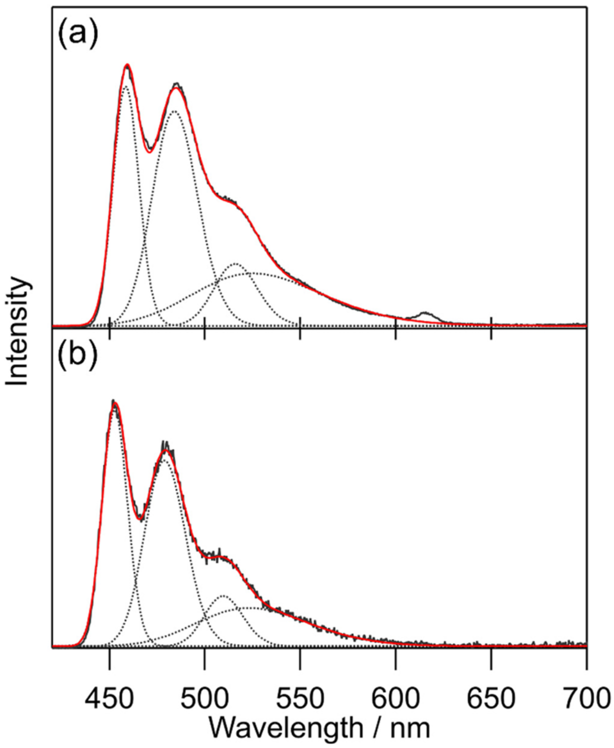

Fig. 4 Phosphorescence spectra (λ_{ex} = 350 nm, 100 K, under vacuum, delay = 20 ms) of the Gd(III) complexes (black lines): (a) [Gd(hfa)$_3$(tppo)$_2$] and (b) [Gd(hfa)$_3$(tcpo)$_2$] with peak deconvolution using the Gaussian function (dotted lines). The red lines are the summations of Gaussian functions.

ively.[1] In the excitation spectra, broad excitation bands attributable to hfa ligands were observed in the ultraviolet region. Emission lifetime (τ_{avg}) and ligand-excited emission quantum yield (Φ_{tot}) were evaluated in air (Table 2). To estimate the hfa ligand T_1 levels, we measured the phosphorescence spectra of [Gd(hfa)$_3$(tppo)$_2$] and [Gd(hfa)$_3$(tcpo)$_2$] (Fig. 4). The phosphorescence spectra were deconvoluted into four vibronic bands and the deconvolution results for the four vibronic bands were designated as 0–0, 0–1, 0–2, and 0–3. The hfa ligand T_1 levels (energy gap $\Delta E_{T1\text{-}5D4}$) were determined based on 0–0 vibronic bands using a wavenumber scale of 21 800 cm^{-1} (1300 cm^{-1}) for [Gd(hfa)$_3$(tppo)$_2$] and 22 100 cm^{-1} (1600 cm^{-1}) for [Gd(hfa)$_3$(tcpo)$_2$].

Back energy transfer (BEnT) under vacuum

We evaluated the value of k_r for [Tb(hfa)$_3$(tppo)$_2$] (k_r = 1.3 × 10^3 s^{-1}) and [Tb(hfa)$_3$(tcpo)$_2$] (k_r = 1.1 × 10^3 s^{-1}) using the emission lifetime at 90 K using a previously reported approximate method.[18,19,43] The variation between k_r values is attributed to the electronic structure differences between [Tb(hfa)$_3$(tppo)$_2$] and [Tb(hfa)$_3$(tcpo)$_2$]. The non-radiative rate constants k_{nr} were estimated based on k_r values and emission decay analyses under vacuum (Fig. S5†). The electronic structure changes also induced a significant difference in k_{nr} values of [Tb(hfa)$_3$(tppo)$_2$] (k_{nr} = 8.8 × 10^3 s^{-1}) and [Tb(hfa)$_3$(tcpo)$_2$] (k_{nr} = 1.0 × 10^3 s^{-1}), indicating that BEnT is inefficient in [Tb(hfa)$_3$(tcpo)$_2$] compared with that in [Tb(hfa)$_3$(tppo)$_2$]. This interpretation is consistent with temperature-dependent emission lifetime measurements under vacuum (Fig. 5). The emission lifetime of [Tb(hfa)$_3$(tppo)$_2$] changed significantly in the lower temperature region, suggesting that BEnT from the $^5D_4$

Table 2 Photophysical parameters of [Tb(hfa)$_3$(tppo)$_2$] and [Tb(hfa)$_3$(tcpo)$_2$]

Entry	k_r [a]/s^{-1} Vacuum	k_{nr} [b]/s^{-1} Vacuum	k_q [c]/s^{-1} —	τ_{avg} [d]/μs Air	Vacuum	O$_2$	Φ_{tot} [e]/% Air	Ar
[Tb(hfa)$_3$(tppo)$_2$]	1.3 × 10^3	8.8 × 10^3	3.8 × 10^2	101 ± 1	105 ± 0.4	82 ± 0.2	9.3 ± 0.3	11.2 ± 0.1
[Tb(hfa)$_3$(tcpo)$_2$]	1.1 × 10^3	1.1 × 10^3	6.2 × 10	453 ± 1	466 ± 1	398 ± 1	31.9 ± 0.1	33.3 ± 0.3

[a] $k_r = 1/\tau_{90\ K}$ (vacuum).[18,19,43] $\tau_{90\ K}$: λ_{ex} = 356 nm, λ_{em} = 542 nm, 90 K. [b] $k_{nr} = 1/\tau$ (vacuum, λ_{ex} = 495 nm) − k_r. [c] $k_q = 1/\tau$ (air) − $1/\tau$ (vacuum). [d] λ_{ex} = 356 nm, λ_{em} = 542 nm, 293 K. It was estimated by fitting with a double-exponential function. The standard deviations were determined by five measurements. [e] λ_{ex} = 370 nm. The standard deviations were determined by measuring five times.

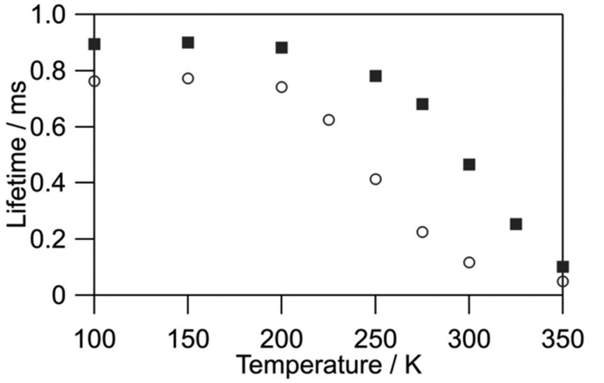

Fig. 5 Temperature-dependent emission lifetimes of [Tb(hfa)$_3$(tppo)$_2$] (circles) and [Tb(hfa)$_3$(tcpo)$_2$] (squares) (λ_{ex} = 356 nm, λ_{em} = 542 nm, under vacuum).

emitting state is more pronounced compared with that of [Tb(hfa)$_3$(tcpo)$_2$]. Under oxygen-free conditions, the ligand-excited emission quantum yield of [Tb(hfa)$_3$(tcpo)$_2$] (Φ_{tot} = 33.3%) was significantly higher than that of [Tb(hfa)$_3$(tppo)$_2$] (Φ_{tot} = 11.2%). This is also ascribed to the suppression of BEnT in [Tb(hfa)$_3$(tcpo)$_2$].

To investigate the BEnT mechanism, we evaluated the emission lifetimes of the Gd(III) complexes. The emission lifetimes under vacuum for [Gd(hfa)$_3$(tppo)$_2$] and [Gd(hfa)$_3$(tcpo)$_2$] were estimated to be 237 and 52 μs, respectively, using emission decay analysis (Fig. S8†). The phosphorescence properties imply that, ideally, [Tb(hfa)$_3$(tppo)$_2$] should show an effective photosensitized Tb(III) emission due to a long-lived T_1 state. However, [Tb(hfa)$_3$(tcpo)$_2$] was found to demonstrate effective photosensitized Tb(III) emission with a larger Φ_{tot}. To further clarify the origins, we evaluated the photophysical properties of the Tb(III) and Gd(III) complexes in the presence of oxygen.

BEnT mechanism in a thermally populated T_1 state during Tb(III) emission

The energy transfer from the T_1 state of an organic ligand to Tb(III) is reversible when the T_1 state is thermally re-populated from the Tb(III) $^5D_4$ state. This re-population of the T_1 state competes with Tb(III) luminescence.[26] When the EnT rate between T_1 and $^5D_4$ states is significantly higher than the deactivation rates of $T_1 \rightarrow S_0$ and $^5D_4 \rightarrow {}^7F_J$ transitions, investigating the oxygen concentration dependence of Tb(III) emission lifetimes is useful for examining the population of the T_1 level during Tb(III) emission.[10,26–31,44]

This measurement relies on the distinct sensitivity property towards O_2, that is the ligand T_1 state exhibits sensitivity to O_2, while the Tb(III) $^5D_4$ state is insensitive to O_2. The decrease of emission lifetimes with the increase of oxygen concentration was observed both in [Tb(hfa)$_3$(tppo)$_2$] and [Tb(hfa)$_3$(tcpo)$_2$] (Table 2, Fig. S5†), revealing the T_1 state population during Tb(III) emission. As indicated by the photophysical analysis of [Gd(hfa)$_3$(tcpo)$_2$] (τ_{avg} = 52 μs), [Tb(hfa)$_3$(tcpo)$_2$] exhibits a shorter T_1 lifetime. Thus, the crucial factor contributing to the emission quantum yield of [Tb(hfa)$_3$(tcpo)$_2$] being higher than that of [Tb(hfa)$_3$(tppo)$_2$] is the difference between EnT and BEnT rates between the two Tb(III) complexes. These energy transfer rate differences between the Tb(III) complexes are attributed to the higher T_1 level of [Tb(hfa)$_3$(tcpo)$_2$] (T_1 = 22 100 cm^{-1}) compared to that of [Tb(hfa)$_3$(tppo)$_2$] (T_1 = 21 800 cm^{-1}). Based on the different 4f–4f radiative rate constant values, the 4f-orbital-based electronic structures of [Tb(hfa)$_3$(tppo)$_2$] and [Tb(hfa)$_3$(tcpo)$_2$] are also different (Table 2). We consider that the 4f-orbital-based electronic structural differences also affect the energy transfer rates. To investigate the effect of the 4f-orbital-based electronic structure on energy transfer rates, the activation energy E_a and frequency factor A in the energy transfer were estimated from an Arrhenius plot using the temperature-dependent emission lifetime (Fig. S7, Table S10†).[45] In particular, the A value, which incorporates electronic frequency, is associated with the electronic coupling of $^5D_4$ with the T_1 state.[46,47] As a consequence, the E_a values were calculated to be identical (2000 cm^{-1}) in Tb(III) complexes, whereas the A values were calculated to be 1.2×10^8 s^{-1} for [Tb(hfa)$_3$(tppo)$_2$] and 1.9×10^7 s^{-1} for [Tb(hfa)$_3$(tcpo)$_2$] (Table S10†). The consistent E_a values stem from a balance between different $\Delta E_{T1\text{-}5D4}$ ([Tb(hfa)$_3$(tppo)$_2$] < [Tb(hfa)$_3$(tcpo)$_2$]) and contrasting T_1 lifetimes ([Tb(hfa)$_3$(tppo)$_2$] > [Tb(hfa)$_3$(tcpo)$_2$]). The smaller A value in [Tb(hfa)$_3$(tcpo)$_2$] indicates less electronic coupling. As $^5D_4$ weakly interacts with the T_1 state in [Tb(hfa)$_3$(tcpo)$_2$], BEnT is passivated, therefore, effective photosensitized Tb(III) emission is observed.

Evaluation of the oxygen barrier ability

Notably, despite the emission quenched by oxygen in the populated T_1 state during Tb(III) emission, [Tb(hfa)$_3$(tcpo)$_2$] exhibits excellent emission properties in air and under oxygen. To elucidate the oxygen barrier ability, the indirect emission quenching constant of oxygen (k_q) was evaluated using the Tb(III) emission lifetimes in air and under vacuum ($k_q = 1/\tau$ (air) $-$ $1/\tau$ (vacuum)). The k_q value of [Tb(hfa)$_3$(tcpo)$_2$] was calculated to be 6.2×10 s^{-1}, significantly smaller than that of [Tb(hfa)$_3$(tppo)$_2$] (3.8×10^2 s^{-1}) (Table 2). The k_q is substantially reduced by the presence of bulky tcpo ligands, which is consistent with the calculated k_q in [Gd(hfa)$_3$(tcpo)$_2$] (Table 3). The energy transfer efficiency is expected to be dependent on the oxygen concentration, although the energy transfer efficiency cannot be estimated precisely at present.[46] It has been reported that quenching of the ligand T_1 state by oxygen originates from orbital overlap between the π-conjugated orbitals of hfa and molecular oxygen.[10] The bulky tcpo ligands inhibit orbital overlapping, providing an oxygen barrier ability (Fig. 6 and S9†). Consequently, we have successfully demonstrated a luminescent Tb(III) complex model in a thermally populated T_1 state with an oxygen barrier system based on ancillary ligands.

Quantum chemical calculations

In photophysical analyses of the Tb(III) complexes, different k_r values were considered to result from the 4f-orbital-based electronic structure differences between [Tb(hfa)$_3$(tppo)$_2$] and [Tb

Table 3 Photophysical parameters of $[Gd(hfa)_3(tppo)_2]$ and $[Gd(hfa)_3(tcpo)_2]$

	$\tau_{avg}{}^{a,b}$/μs				
Entry	Air	Vacuum	O_2	k_q/s^{-1}	T_1 level^c/ cm^{-1}
$[Gd(hfa)_3(tppo)_2]$	64 ± 1	237 ± 1	16 ± 0.2	1.1×10^4	21 800
$[Gd(hfa)_3(tcpo)_2]$	50 ± 0.3	52 ± 0.5	29 ± 0.2	7.3×10^2	22 100

[a] λ_{ex} = 355 nm, λ_{em} = 500 nm (using a 510 nm short-pass filter with a 490 nm long-pass filter), 293 K. [b] It was estimated by fitting with a double-exponential function. The standard deviations were determined by ten measurements. [c] Estimated from phosphorescence spectra.

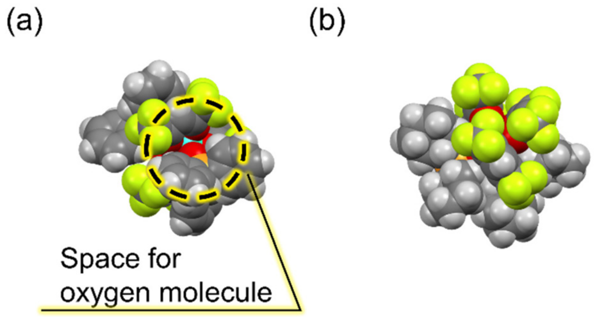

Fig. 6 Space-fill drawing models of (a) $[Tb(hfa)_3(tppo)_2]$ and (b) $[Tb(hfa)_3(tcpo)_2]$.

$(hfa)_3(tcpo)_2]$. The 4f–4f transition characteristics are affected by ligand polarization[48–53] and/or the charge transfer excited state between the π-orbital and the 4f-orbital.[54,55] According to the dynamic coupling model, the 4f–5d excited states are mixed with the 4f–4f excited state by the interaction between the induced electronic dipole moment of the ligands and the transition electric quadrupole moment of the lanthanide. Thus, the 4f–4f oscillator strength f depends on the ligand polarizability, and can be approximately described as follows:[56]

$$f \propto \alpha^2 R^{-8} \tag{1}$$

where α and R are the ligand polarizability and the distance between the coordination atom and lanthanide ion, respectively. To further clarify the Tb(III) 4f-orbital-based electronic structural differences, the quantum chemical calculations were performed for $[Tb(hfa)_3(tppo)_2]$ and $[Tb(hfa)_3(tcpo)_2]$ using crystal structures (ULC-BLYP/Stuttgart RSC 1997 for Tb atoms, cc-pVDZ for C, H, O, F, and P atoms).[35–38] The summation of the α^2R^{-8} value of $[Tb(hfa)_3(tppo)_2]$ did not differ from that of $[Tb(hfa)_3(tcpo)_2]$ (Table S13†).

In contrast, Henrie reported an equation for the 4f–4f oscillator strength f_{pt} borrowed from the charge-transfer (CT) transition between the π and 4f orbitals as follows:[54]

$$f_{pt} \propto E_{CT}{}^{-3} f_{CT} \tag{2}$$

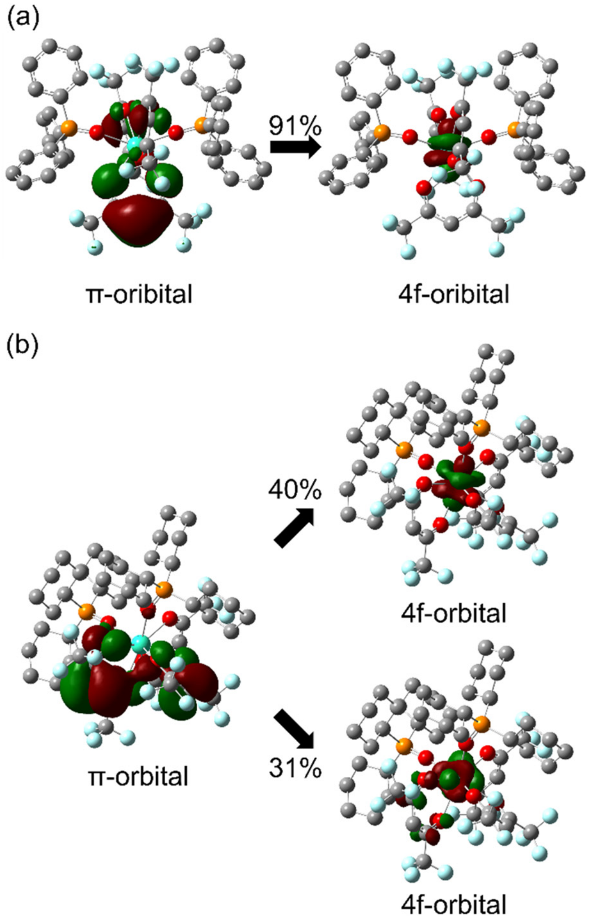

Fig. 7 Molecular orbital characteristics of the lowest LMCT transition of Tb(III) complexes: (a) $[Tb(hfa)_3(tppo)_2]$ and (b) $[Tb(hfa)_3(tcpo)_2]$.

where E_{CT} and f_{CT} are the excitation energy of the CT state and the oscillator strength of the CT transition, respectively. The lowest energy level in the CT transition originates from the ligand (π-orbital) to metal (4f-orbital) charge transfer (LMCT) transition (Fig. 7, Tables S14 and S15†). The 4f-orbital shapes depend on the coordination geometry. The average of calculated parameter ($E_{CT}{}^{-3}f_{CT}$) of $[Tb(hfa)_3(tppo)_2]$ (1.05×10^{-16} cm^3) is significantly larger than that of $[Tb(hfa)_3(tcpo)_2]$ (1.11×10^{-17} cm^3) (Table 4). The differences in the k_r values and EnT rate of the Tb(III) complexes might be attributed to the electronic structure difference in the perturbations of the LMCT states to the 4f–4f states, in addition to the difference in the coordination geometry.

Conclusion

In this study, an effective photosensitized emission was demonstrated by fabricating a Tb(III) complex with a typical hexafluoroacetylacetonate photosensitizer in the thermally populated T_1 state. The bulky ancillary ligand structure acts as a modulator of the 4f-orbital-based electronic structure and an oxygen barrier to suppress orbital overlap between the

Table 4 Parameters expressing the contribution of the LMCT state with respect to the 4f–4f states of the Tb(III) complexes for oscillator strength of the 4f–4f transition

Entry	$E_{\mathrm{CT}}{}^{-3}f_{\mathrm{CT}}{}^{a}$/cm^3
[Tb(hfa)$_3$(tppo)$_2$]	1.05×10^{-16}
[Tb(hfa)$_3$(tcpo)$_2$]	1.11×10^{-17}

[a] Average of the approximate parameters calculated from excitation energies and oscillator strengths for the bottom 20 LMCT levels (Tables S14 and S15†).

β-diketonate photosensitizer and molecular oxygen. These results provide new insights into the photosensitizer model based on thermally populated T_1 states during Tb(III) emission for the improvement of brightness in luminescent Tb(III) complexes in the presence of oxygen, such as in air. Studies on oxygen barrier control methods using polyaromatic photosensitizers for bright lanthanide emission[25] are currently in progress.

Author contributions

Yuichi Kitagawa designed this research. Kota Inage performed all the syntheses, optical measurements, and structural analyses and wrote the paper. Kota Inage, Mengfei Wang, Yasuchika Hasegawa, and Yuichi Kitagawa discussed this work. All the authors have reviewed the final version of the paper.

Conflicts of interest

The authors declare no conflict of interest.

Acknowledgements

This work was partially supported by a grant-in-aid with JSPS KAKENHI Grant Numbers JP20H02748, JP20H04653, JP20H05197, JP20K21201, JP21K18969, JP22H02152, JP22H04516, and JP23K17925. This work is supported by the Adaptable and Seamless Technology Transfer Program through Target-driven R&D (A-STEP) from the Japan Science and Technology Agency (JST), Japan Grant Number JPMJTR23T5. This work was also supported by the Institute for Chemical Reaction Design and Discovery (ICReDD), established by the World Premier International Research Center Initiative (WPI) of the MEXT, Japan.

References

1 J.-C. G. Bünzli, *Chem. Rev.*, 2010, **110**, 2729–2755.
2 K. Binnemans, *Chem. Rev.*, 2009, **109**, 4283–4374.
3 J.-C. G. Bünzli, *Coord. Chem. Rev.*, 2015, **293–294**, 19–47.
4 A. B. Dias, *Dalton Trans.*, 2007, 2229–2241.
5 L. Wang, Z. Zhao, C. Wei, H. Wei, Z. Liu, Z. Bian and C. Huang, *Adv. Opt. Mater.*, 2019, **7**, 1801256.
6 N. Sun, L. Li, Y. Yang, A. Zhang, H. Jia, X. Liu and B. Xu, *Opt. Mater.*, 2015, **49**, 39–45.
7 S. F. H. Correia, R. L. Fernandes, L. Fu, M. M. Nolasco, L. D. Carlos and R. A. S. Ferreira, *Eur. J. Inorg. Chem.*, 2020, **2020**, 1736–1742.
8 C. D. S. Brites, S. Balabhadra and L. D. Carlos, *Adv. Opt. Mater.*, 2019, **7**, 1801239.
9 K. Miyata, Y. Konno, T. Nakanishi, A. Kobayashi, M. Kato, K. Fushimi and Y. Hasegawa, *Angew. Chem., Int. Ed.*, 2013, **52**, 6413–6413.
10 Y. Kitagawa, T. Nakai, S. Hosoya, S. Shoji and Y. Hasegawa, *ChemPlusChem*, 2023, **88**, e202200445.
11 K. Iman and M. Shahid, *New J. Chem.*, 2019, **43**, 1094–1116.
12 D. Parker, J. D. Fradgley and K. L. Wong, *Chem. Soc. Rev.*, 2021, **50**, 8193–8213.
13 D. Parker, *Coord. Chem. Rev.*, 2000, **205**, 109–130.
14 Z. Gao, B. Xu, T. Zhang, Z. Liu, W. Zhang, X. Sun, Y. Liu, X. Wang, Z. Wang, Y. Yan, F. Hu, X. Meng and Y. S. Zhao, *Angew. Chem., Int. Ed.*, 2020, **59**, 19060–19064.
15 Z. Gao, S. Yang, B. Xu, T. Zhang, S. Chen, W. Zhang, X. Sun, Z. Wang, X. Wang, X. Meng and Y. S. Zhao, *Angew. Chem., Int. Ed.*, 2021, **60**, 24519–24525.
16 J. Andres, R. D. Hersch, J. E. Moser and A. S. Chauvin, *Adv. Funct. Mater.*, 2014, **24**, 5029–5036.
17 M. Latva, H. Takalo, V.-M. Mukkala, C. Matachescu, J. C. Rodriguez-Ubis and J. Kankare, *J. Lumin.*, 1997, **75**, 149–169.
18 A. R. Ramya, M. L. P. Reddy, A. H. Cowley and K. V. Vasudevan, *Inorg. Chem.*, 2010, **49**, 2407–2415.
19 K. Yanagisawa, T. Nakanishi, Y. Kitagawa, T. Seki, T. Akama, M. Kobayashi, T. Taketsugu, H. Ito, K. Fushimi and Y. Hasegawa, *Eur. J. Inorg. Chem.*, 2015, **2015**, 4769–4774.
20 P. R. Matthes, J. Nitsch, A. Kuzmanoski, C. Feldmann, A. Steffen, T. B. Marder and K. Müller-Buschbaum, *Chem. – Eur. J.*, 2013, **19**, 17369–17378.
21 A. S. Souza, L. A. Nunes, M. C. F. C. Felinto, H. F. Brito and O. L. Malta, *J. Lumin.*, 2015, **167**, 167–171.
22 A. N. C. Neto, E. Kasprzycka, A. S. Souza, P. Gawryszewska, M. Suta, L. D. Carlos and O. L. Malta, *J. Lumin.*, 2022, **248**, 118933.
23 Y. Kitagawa, F. Suzue, T. Nakanishi, K. Fushimi, T. Seki, H. Ito and Y. Hasegawa, *Commun. Chem.*, 2020, **3**, 3.
24 Y. Kitagawa, R. Moriake, T. Akama, K. Saito, K. Aikawa, S. Shoji, K. Fushimi, M. Kobayashi, T. Taketsugu and Y. Hasegawa, *ChemPlusChem*, 2022, **87**, e202200151.
25 Y. Kitagawa, K. Shima, T. Nakai, M. Kumagai, S. Omagari, P. P. Ferreira da Rosa, S. Shoji, K. Fushimi and Y. Hasegawa, *Commun. Chem.*, 2023, **6**, 122.
26 N. Sabbatini, M. Guardigli, I. Manet, F. Bolletta and R. Ziessel, *Inorg. Chem.*, 1994, **33**, 955–959.
27 A. Beeby, D. Parker and J. A. G. Williams, *J. Chem. Soc., Perkin Trans. 2*, 1999, **2**, 493–504.

28 S. Blair, R. Kataky and D. Parker, *New J. Chem.*, 2002, **26**, 530–535.

29 G. L. Law, R. Pal, L. O. Palsson, D. Parker and K. L. Wong, *Chem. Commun.*, 2009, 7321–7323.

30 J. Lehr, M. Tropiano, P. D. Beer, S. Faulkner and J. J. Davis, *Chem. Commun.*, 2015, **51**, 15944–15947.

31 T. J. Sørensen, A. M. Kenwright and S. Faulkner, *Chem. Sci.*, 2015, **6**, 2054–2059.

32 S. Katagiri, Y. Tsukahara, Y. Hasegawa and Y. Wada, *Bull. Chem. Soc. Jpn.*, 2007, **80**, 1492–1503.

33 O. V. Dolomanov, L. J. Bourhis, R. J. Gildea, J. A. K. Howard and H. Puschmann, *J. Appl. Crystallogr.*, 2009, **42**, 339–341.

34 G. M. Sheldrick, *Acta Cryst. A*, 2008, **64**, 112–122.

35 M. J. Frisch, G. W. Trucks, H. B. Schlegel, G. E. Scuseria, M. A. Robb, J. R. Cheeseman, G. Scalmani, V. Barone, G. A. Petersson, H. Nakatsuji, X. Li, M. Caricato, A. V. Marenich, J. Bloino, B. G. Janesko, R. Gomperts, B. Mennucci, H. P. Hratchian, J. V. Ortiz, A. F. Izmaylov, J. L. Sonnenberg, D. Williams-Young, F. Ding, F. Lipparini, F. Egidi, J. Goings, B. Peng, A. Petrone, T. Henderson, D. Ranasinghe, V. G. Zakrzewski, J. Gao, N. Rega, G. Zheng, W. Liang, M. Hada, M. Ehara, K. Toyota, R. Fukuda, J. Hasegawa, M. Ishida, T. Nakajima, Y. Honda, O. Kitao, H. Nakai, T. Vreven, K. Throssell, J. A. Montgomery Jr., J. E. Peralta, F. Ogliaro, M. J. Bearpark, J. J. Heyd, E. N. Brothers, K. N. Kudin, V. N. Staroverov, T. A. Keith, R. Kobayashi, J. Normand, K. Raghavachari, A. P. Rendell, J. C. Burant, S. S. Iyengar, J. Tomasi, M. Cossi, J. M. Millam, M. Klene, C. Adamo, R. Cammi, J. W. Ochterski, R. L. Martin, K. Morokuma, O. Farkas, J. B. Foresman and D. J. Fox, *Gaussian 16, Revision C.01*, Gaussian, Inc., Wallin, 2016.

36 M. Dolg, H. Stoll, A. Savin and H. Preuss, *Theor. Chim. Acta*, 1989, **75**, 173–194.

37 B. P. Pritchard, D. Altarawy, B. Didier, T. D. Gibson and T. L. Windus, *J. Chem. Inf. Model.*, 2019, **59**, 4814–4820.

38 T. H. Dunning, *J. Chem. Phys.*, 1989, **90**, 1007–1023.

39 K. Miyata, T. Nakagawa, R. Kawakami, Y. Kita, K. Sugimoto, T. Nakashima, T. Harada, T. Kawai and Y. Hasegawa, *Chem. – Eur. J.*, 2011, **17**, 521–528.

40 *SHAPE, version 2.1. Continuous shape measures calculations. Electronic Structure Group*, Universitat de Barcelona, Spain, 2010.

41 D. Casanova, M. Llunell, P. Alemany and S. Alvarez, *Chem. – Eur. J.*, 2005, **11**, 1479–1494.

42 M. Pinsky and D. Avnir, *Inorg. Chem.*, 1998, **37**, 5575–5582.

43 R. Pavithran, N. S. S. Kumar, S. Biju, M. L. P. Reddy, S. A. Junior and R. O. Freire, *Inorg. Chem.*, 2006, **45**, 2184–2192.

44 R. Hueting, M. Tropiano and S. Faulkner, *RSC Adv.*, 2014, **4**, 44162–44165.

45 K. Yanagisawa, Y. Kitagawa, T. Nakanishi, T. Akama, M. Kobayashi, T. Seki, K. Fushimi, H. Ito, T. Taketsugu and Y. Hasegawa, *Eur. J. Inorg. Chem.*, 2017, **2017**, 3843–3848.

46 S. Omagari and M. Vacha, *Phys. Chem. Chem. Phys.*, 2020, **22**, 3683–3690.

47 V. M. Korshunov, M. A. Kiskin and I. V. Taydakov, *J. Lumin.*, 2022, **251**, 119235.

48 R. D. Peacock, *J. Mol. Struct.*, 1978, **46**, 203–207.

49 S. F. Mason, R. D. Peacock and B. Stewart, *Chem. Phys. Lett.*, 1974, **29**, 149–153.

50 M. F. Reid and F. Richardson, *J. Phys. Chem.*, 1984, **88**, 3579–3586.

51 M. F. Reid and F. S. Richardson, *J. Chem. Phys.*, 1983, **79**, 5735–5742.

52 L. Hu, M. F. Reid, C.-K. Duan, D. J. Newman and G. Balasubramanian, *J. Phys. C: Solid State Phys.*, 1975, **8**, 37–44.

53 M. F. Reid and F. S. Richardson, *Chem. Phys. Lett.*, 1983, **95**, 113–118.

54 D.-E. Henrie, R.-L. Fellows and G. R. Choppin, *Coord. Chem. Rev.*, 1976, **18**, 199–224.

55 Y. Kitagawa, P. P. Ferreira Da Rosa and Y. Hasegawa, *Dalton Trans.*, 2021, **50**, 14978–14984.

56 M. Hatanaka and S. Yabushita, *Chem. Phys. Lett.*, 2011, **504**, 193–198.